ACADEMIC PRESS

Available online at www.sciencedirect.com

SCIENCE DIRECT®

Journal of Sound and Vibration 261 (2003) 675–696

JOURNAL OF SOUND AND VIBRATION

www.elsevier.com/locate/jsvi

Coupled transverse and axial vibratory behaviour of cracked beam with end mass and rotary inertia

M.H.F. Dado*, O. Abuzeid

Department of Mechanical Engineering. University of Jordan, Amman 11943, Jordan

Received 30 November 2001; accepted 23 April 2002

Abstract

In this paper the vibrational behaviour of a cracked cantilever beam carrying end mass and rotary inertia is investigated. The transverse and axial vibrations of the beam are coupled through the crack model. The values of the ratio between the cracked and uncracked beam natural frequencies, the frequency ratio, are examined and are shown to follow well-defined trends with respect to the crack parameters and end mass and rotary inertia. However, the coupling between the transverse and axial vibrations is shown to be weak for the first two modes for moderate values of crack depth ratio. High crack depth ratios appear to increase the coupling effects. Low aspect ratios are expected to show strong coupling effects and further investigation is recommended using Timoshenko beam theory.

1. Introduction

Beams are one of the most commonly used structural elements in numerous engineering applications and thus experience a wide variety of static and dynamic loads. It is well known that in design one assumes material properties not to vary throughout the presumed life of a beam, but there are many situations in practice in which these properties would change because of continuous wear and friction suffered during operation. This occurs in particular when the component is designed to take loads near or beyond the material yield load [1]. However, even if the area under damage is too small to endanger the overall structural integrity and reliability, its influence on the dynamic characteristics could be important.

Considering the crack as a significant form of such damage, its modelling is an important step in studying the behaviour of damaged structures. Knowing the crack compliance, the beam or

*Corresponding author. Tel.: +962-6-535-5000x2768; fax: +962-6-535-558.
E-mail address: dado@ju.edu.jo (M.H.F. Dado).

0022-460X/03/$ - see front matter
doi:10.1016/S0022-460X(02)01004-0

shaft can be modelled using either Euler–Bernoulli or Timoshenko beam theories. The beam boundary conditions are used along with the crack compatibility relations to derive the characteristic equation relating the natural frequency, the crack depth and location with the other beam properties.

The earliest attempts to identify the stiffness discontinuities in beams date back to 1949, when the influence of a small slot on the free vibration of a uniform beam was studied by Thompson [2], although this reduction in area does not truly represent local material damage. The growth or coalesence of micro-cracks under repeated loading is another case in which a local flexibility is introduced in [3], which for a beam can be described by way of a local flexibility matrix, the dimension of which depends on the number of degrees of freedom considered (maximum 6×6). Such a matrix was introduced first for beams of rectangular cross-section with transverse surface cracks by Dimarogonas and Paipeties [4] for five degrees of freedom neglecting torsion. The influence of an edge crack of a specified size on the vibration of a circular shaft has been studied by Dimarogonas and Papadopoulos [5]. Chondros et al. [6] and Chondros and Dimarogonas [7] studied the vibration of cracked beams with simply supported and cantilever boundary conditions, respectively. The Hu–Washizu–Barr variational formulation was used to develop the differential equation and the boundary conditions of the cracked beams. They compared the local flexibility method with the continuous system, the decaying stress field, and the experimental results of thin slots in place of cracks. The results were all in good agreement. A 2×2 local flexibility matrix with the coupling terms have been modelled analytically by Papadopoulos and Dimarogonas [3]. The prediction of mixed mode crack initiation and propagation direction was considered by Nobile [8] utilizing the S-theory developed by Sih [9]. The S-theory could be used as an alternative approach to model the flexibility matrix of single and mixed mode cracks. The measured vibration amplitude was related to the crack location and depth by Rizos et al. [10], in which the crack was represented by a bending spring utilizing the approach proposed by Dimarogonas and Paipeties [4]. An equation of bending motion for Euler–Bernoulli beam containing pairs of symmetrical open cracks was derived by Christides and Barr [11]. The cracks were considered to be normal to the beam's neutral axis and symmetrical about the plane of bending. An approximate Galerkin solution to model a beam with a pair of cracks symmetrically located about the neutral axis was developed by Shen and Pierre [12] in which a theory developed by Christides and Barr [11] was employed. An expression for the natural frequency of a beam containing two open cracks was developed by Joshi and Madhusudhan [1]. Their expression predicts the change of natural frequency for the first five natural modes of vibration for a beam with four different boundary conditions. Analytical expressions and plots relating the crack depth and location of cracked Timoshenko shaft for the first few natural frequencies of the shaft have been developed by Rajab and Al-Saleeh [13]. These expressions were obtained by modelling the crack as bending and shear compliance of equivalent incremental strain energy by using the J-integral concept from fracture mechanics. It was shown that knowledge of the relative change in the first three natural frequencies is enough to estimate the crack depth and crack location in the shaft. The slenderness ratio effect on a cracked beam was investigated by Kikidis and Papadopoulos [14]. They showed that the slenderness ratio has a significant effect on the coupled bending and torsional vibration. They compared the behaviour of a model based on Euler–Bernoulli beam theory and a model based on Timoshenko beam theory. The perturbation method and finite element method were used by Gudmundson [15,16] to predict the changes in resonance

frequencies of structural members due to cracks or any geometrical changes. An experimental and analytical investigation were carried out by Ismail et al. [17] in their study of fatigue crack identification using vibration testing. They modelled the crack using a combination of torsional and shear springs. They pointed out that calculations based only on the drop of natural frequencies of higher modes may lead to an underestimation of the crack severity. An algorithm was developed by Dado [18] to predict the depth and location of an open transverse crack in a beam with rectangular cross-section with four different boundary conditions, in which the model developed by Dimarogonas and Paipeties [4] has been extended. This algorithm requires the natural frequencies of the first two modes of vibration of the cracked beam to enter tables of model generated data. A method for modelling transverse vibration of geometrically segmented slender beams of constant thickness with and without crack exploiting the Frobenius technique was proposed by Chaudhari et al. [19]. A comparison with a finite element solution was resorted to and a maximum of 3% error was recorded in predicting the crack location. A finite element model for a tapered rotating cracked shaft for the modal analysis and dynamic modelling of rotor-bearing systems was developed by Mohiuddin and Khulief [20]. The formulation of the tapered rotating cracked shaft included shear deformation and rotary inertia. The coupling between the axial load and the crack depth of a cracked fixed–fixed beam was studied by Masoud et al. [21]. It was found that the natural frequency could not be determined by a simple superposition of the axial load and crack depth effects. The coupling significance was found to be directly proportional to the crack depth and axial load. The effect of a crack on the dynamic stability of a free–free Timoshenko beam subjected to a constant or a pulsating follower force was studied by Kim and Kim [22]. A mathematical model for the crack was introduced in the form of the bending and shear compliance of equivalent incremental strain energy.

This paper presents a modelling and analysis algorithm for cracked Euler–Bernoulli beams by considering the coupling between the bending and axial modes of vibration. The beam is a cantilever with a rectangular cross-section. The algorithm studies the vibrational behaviour of the cracked beam, and particularly the natural frequency and mode shapes under the effect of added mass and rotary inertia at the free end. The crack compliance is modelled using the strain energy release rate relation. Polynomial regression relations are obtained and implemented in modelling the crack compliance 2×2 matrix.

2. The cracked beam model

The cracked beam is modelled as two continuous segments that are coupled by the crack compliance matrix. The equation that governs the longitudinal motion of a uniform elastic beam segment can be expressed as

$$EA \frac{\partial^2 u(x,t)}{\partial x^2} - \bar{m} \frac{\partial^2 u(x,t)}{\partial t^2} = 0 \tag{1}$$

and the equation that governs the transverse motion of a uniform elastic *Euler–Bernoulli* beam segment can be expressed as

$$EI \frac{\partial^4 v(x,t)}{\partial x^4} + \bar{m} \frac{\partial^2 v(x,t)}{\partial t^2} = 0, \tag{2}$$

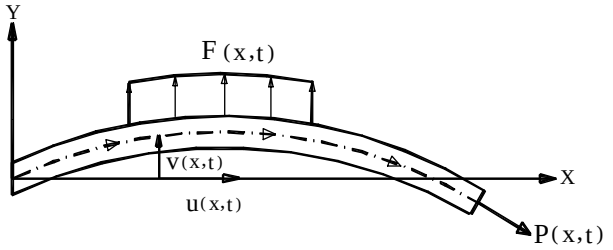

Fig. 1. Beam under axial and transverse loading.

where $u(x,t)$ and $v(x,t)$ are the axial and transverse displacements of a point along the beam as shown in Fig. 1. $\bar{m}$ is the mass per unit length (kg/m), E is the modulus of elasticity (N/m^2), and I is the area moment of inertia (m^4).

Using the method of separation of variables, the solution in the spatial domain for the governing equations is given as

$$\frac{\mathrm{d}^2U(x)}{\mathrm{d}x^2}+\frac{\omega^2\bar{m}}{EA}U(x)=0 \tag{3}$$

and

$$\frac{\mathrm{d}^4V(x)}{\mathrm{d}x^4}+\frac{\omega^2\bar{m}}{EI}V(x)=0. \tag{4}$$

Let

$$k_u^2=\frac{\omega^2\bar{m}L^2}{EA}, \tag{5}$$

$$k_v^4=\frac{\omega^2\bar{m}L^4}{EI}, \tag{6}$$

where L is the total length of the beam and ω is known as the natural frequency of the beam.

The general solutions for Eqs. (3) and (4) are

$$U(x)=C_1\cos(k_u\bar{x})+C_2\sin(k_u\bar{x}), \tag{7}$$

$$V(x)=C_3\cos(k_v\bar{x})+C_4\sin(k_v\bar{x})+C_5\cosh(k_v\bar{x})+C_6\sinh(k_v\bar{x}), \tag{8}$$

where $\bar{x}=x/L$.

Consider the cracked beam model shown in Fig. 2. The spatial domain equation for the segment $0\leqslant x<x_c$ could be written using the forms in Eqs. (7) and (8) as

$$U_1(x)=A_1\cos(k_u\bar{x})+A_2\sin(k_u\bar{x}), \tag{9}$$

$$V_1(x)=A_3\cos(k_v\bar{x})+A_4\sin(k_v\bar{x})+A_5\cosh(k_v\bar{x})+A_6\sinh(k_v\bar{x}) \tag{10}$$

and that for the segment $x_c\leqslant x\leqslant L$ is written as

$$U_2(x)=A_7\cos(k_u\bar{x})+A_8\sin(k_u\bar{x}), \tag{11}$$

$$V_2(x)=A_9\cos(k_v\bar{x})+A_{10}\sin(k_v\bar{x})+A_{11}\cosh(k_v\bar{x})+A_{12}\sinh(k_v\bar{x}). \tag{12}$$

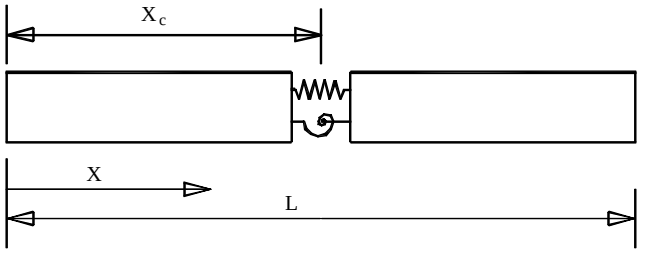

Fig. 2. Two-segment cracked beam model.

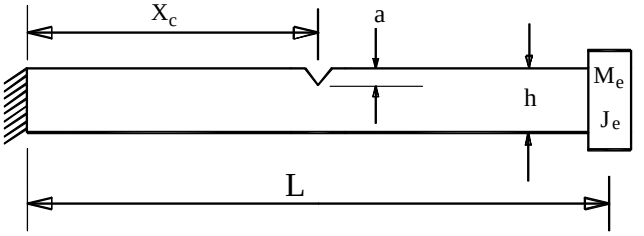

Fig. 3. Cantilever beam with concentrated mass and rotary inertia.

The internal axial force P and bending moment M at the crack are expressed as

$$\begin{Bmatrix} P \\ M \end{Bmatrix} = \begin{bmatrix} k_{11} & k_{12} \\ k_{21} & k_{22} \end{bmatrix} \begin{Bmatrix} U_2(x_c) - U_1(x_c) \\ V_2'(x_c) - V_1'(x_c) \end{Bmatrix}, \tag{13}$$

where k_{ij} are the elements of the stiffness matrix equivalent to the crack. This matrix is derived in Section 3 of this paper. P and M are given in terms of the beam elastic deflections as

$$\begin{Bmatrix} P \\ M \end{Bmatrix} = \begin{Bmatrix} EAU'(x_c) \\ EIV''(x_c) \end{Bmatrix}. \tag{14}$$

Combining Eqs. (13) and (14) provides two equations for relating the coefficients A_1–A_{12}. In addition, the continuity relations at the crack provide the following equations:

$$U_1'(x_c) = U_2'(x_c), \tag{15a}$$

$$V_1(x_c) = V_2(x_c), \tag{15b}$$

$$V_1''(x_c) = V_2''(x_c), \tag{15c}$$

$$V_1'''(x_c) = V_2'''(x_c). \tag{15d}$$

The boundary conditions for the cantilever beam with a concentrated mass and rotary inertia at the free end (Fig. 3) are

$$U_1(0) = 0, \quad U_2'(L) = -\frac{M_r k_u^2}{L} U_2(L), \tag{16a}$$

$$V_1(0) = 0, \quad V_2'''(L) = -\frac{M_r k_v^4}{L^3} V_2(L), \tag{16b}$$

$$V_1'(0) = 0, \quad V_2''(L) = \frac{J_r k_v^4}{L} V_2'(L), \tag{16c}$$

where M_r is the concentrated mass ratio given by

$$M_r = \frac{M_e}{\bar{m}L} \tag{17}$$

and J_r is the rotary inertia ratio given by

$$J_r = \frac{J_e}{\bar{m}L^3}, \tag{18}$$

where M_e and J_e are the concentrated mass and the rotary inertia added at the free end.

3. Crack stiffness matrix

The presence of a transverse through the thickness crack of depth a introduces a local flexibility matrix, the dimension of which depends on the degrees of freedom considered in the problem. In the case of axial and bending loads, the matrix is only (2×2), as each side has two degrees of freedom where the off-diagonal elements of the matrix are considered as coupling elements in the flexibility matrix.

The elastic strain energy release rate, G, could be expressed as follows:

$$G = \frac{1 - v^2}{E}(K_{IP} + K_{IM})^2, \tag{19}$$

where v is the Poisson ratio, and E is the modulus of elasticity. K_{IP} and K_{IM} are the stress intensity factors of mode I (the opening of the crack) for axial force P and bending moment M, respectively. To guarantee the open crack mode, the beam is assumed to be preloaded by its own weight. The amplitude of vibration is assumed to be well below the crack opening due to preloading. The stress intensity factors from elementary fracture mechanics are given as

$$K_{IP} = \frac{P}{bh}(\pi\alpha)^{1/2} F_1, \tag{20}$$

$$K_{IM} = \frac{6M}{bh^2}(\pi\alpha)^{1/2} F_2, \tag{21}$$

where b and h are the cross-section dimensions and α is the crack depth as shown in Fig. 4.

The functions F_1 and F_2 are dependent on the crack depth α and are approximated (as proposed by Ewalds and Wnahil [23]) by

$$F_1 = \sqrt{\frac{2\tan(\pi\alpha/2)}{\pi\alpha}}\left(\frac{0.752 + 2.02\alpha + 0.37(1.0 - \sin(\pi\alpha/2))^3}{\cos(\pi\alpha/2)}\right), \tag{22}$$

$$F_2 = \frac{1.99 - \alpha(1 - \alpha)(2.15 - 3.39\alpha + 2.7\alpha^2)}{\sqrt{\pi}(1 + 2\alpha)(1 - \alpha)^{3/2}}. \tag{23}$$

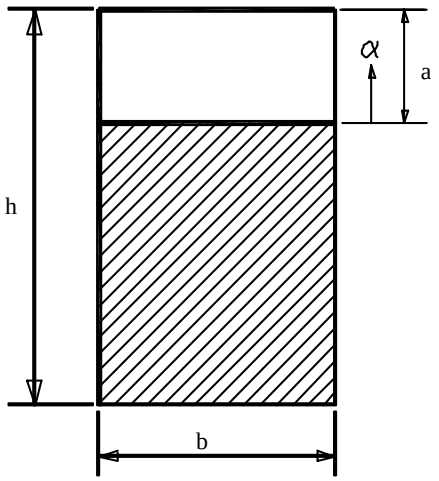

Fig. 4. Geometry of the cracked section of the cantilever beam.

For a rectangular strip with unit width, the local axial, coupled axial and bending, and bending compliance are defined, respectively, as proposed by Dimarogonas and Papadopoulos [5] by

$$c'_{11} = \frac{\partial^2}{\partial P^2}\int_0^a G\,\mathrm{d}\alpha, \tag{24}$$

$$c'_{12} = c'_{21} = \frac{\partial^2}{\partial P \partial M}\int_0^a G\,\mathrm{d}\alpha, \tag{25}$$

$$c'_{22} = \frac{\partial^2}{\partial M^2}\int_0^a G\,\mathrm{d}\alpha, \tag{26}$$

where a is the maximum crack depth as shown in Fig. 4.

Defining the dimensionless parameters $\bar{\alpha} = \alpha/h$ and $\bar{a} = a/h$, the compliance coefficients for the full beam width could be written as

$$c_{11} = \frac{2\pi h}{A}\frac{(1-\nu^2)}{E}\int_0^{\bar{a}} \bar{\alpha} F_1^2(\bar{\alpha})\,\mathrm{d}\bar{\alpha}, \tag{27}$$

$$c_{12} = c_{21} = \frac{\pi h^2}{I}\frac{(1-\nu^2)}{E}\int_0^{\bar{a}} \bar{\alpha} F_1(\bar{\alpha}) F_2(\bar{\alpha})\,\mathrm{d}\bar{\alpha}, \tag{28}$$

$$c_{22} = \frac{6\pi h}{I}\frac{(1-\nu^2)}{E}\int_0^{\bar{a}} \bar{\alpha} F_2^2(\bar{\alpha})\,\mathrm{d}\bar{\alpha}, \tag{29}$$

where $A = bh$ and $I = bh^3/12$ are the cross-sectional area and the area moment of inertia.

The integrals in Eqs. (27)–(29) are evaluated numerically using 16 point quadrature formulae. The results are fitted to polynomial expressions for the three compliance factors using $\bar{a}$ as the

independent variable. The polynomial expressions are found as follows:

$$c_{11} = \frac{2\pi h}{A}\frac{(1-\nu^2)}{E}(0.005777459 + 0.1010004\bar{a} - 4.137205\bar{a}^2 + 35.37731\bar{a}^3 - 89.41206\bar{a}^4 + 83.65015\bar{a}^5), \tag{30}$$

$$c_{12} = \frac{\pi h^2}{I}\frac{(1-\nu^2)}{E}(0.002143934 + 0.0384199\bar{a} - 1.171652\bar{a}^2 + 12.8375\bar{a}^3 - 32.61926\bar{a}^4 + 31.34015\bar{a}^5), \tag{31}$$

$$c_{22} = \frac{6\pi h}{I}\frac{(1-\nu^2)}{E}(0.000537323 + 0.026002454\bar{a} - 0.1846979\bar{a}^2 + 4.526204\bar{a}^3 - 11.76326\bar{a}^4 + 11.64832\bar{a}^5) \tag{32}$$

in which the correlation coefficients are more than 0.99.

The crack stiffness matrix used in Eq. (13) is defined as

$$\begin{bmatrix} k_{11} & k_{12} \\ k_{21} & k_{22} \end{bmatrix} = \begin{bmatrix} c_{11} & c_{12} \\ c_{21} & c_{22} \end{bmatrix}^{-1} \tag{33}$$

or, $k_{11} = c_{22}/\Delta$, $k_{12} = -c_{12}/\Delta$, $k_{21} = -c_{12}/\Delta$, $k_{22} = c_{11}/\Delta$, and $\Delta = c_{11}c_{22} - c_{12}c_{21}$, and the non-dimensional stiffness matrix elements as

$$\bar{k}_{11} = \frac{h}{EA}k_{11}, \quad \bar{k}_{12} = \frac{k_{12}}{EA} \quad \text{and} \quad \bar{k}_{22} = \frac{h}{EI}k_{22}. \tag{34}$$

4. Frequency ratio evaluation and mode shape determination

The natural frequency of the cracked beam could be evaluated using the crack model and the beam continuity and boundary conditions. Eqs. (13)–(16) define these relations as a set of 12 homogenous linear simultaneous algebraic equations. These equations could be written in compact form as

$$[\mathbf{B}]\{\mathbf{A}\} = \{\mathbf{0}\}, \tag{35}$$

where [**B**] is the coefficient matrix defined in terms of the cracked beam parameters and given in Appendix A. The vector $\{\mathbf{A}\} = [A_1, \ldots, A_{12}]^{\mathrm{T}}$ contains the coefficients used in Eqs. (9)–(12). For non-trivial values for the vector {**A**}, Eq. (35) leads to the following characteristic equation:

$$|\mathbf{B}| = 0. \tag{36}$$

Given all the cracked beam parameters, the only unknown in Eq. (36) is the value of the natural frequency ω. The secant method for numerically finding the roots of a non-linear equation is implemented. The frequency of the identical uncracked beam is easily obtained by modifying Eq. (36), where the crack relations are removed and only the equations describing the boundary conditions are applied resulting in a 6×6 characteristic matrix.

The mode shapes for the transverse and axial vibration are determined by evaluating the vector $\{\mathbf{A}\} = [A_1, \ldots, A_{12}]^{\mathrm{T}}$. This is done by setting the value of one of the elements of {**A**} to 1.0, in this

case element A_{12}, and then solving for the rest of the elements using Eq. (35) after the required modifications. From the mode shape analysis, the extent of coupling between transverse and axial vibration is determined. The results are discussed in the following section.

5. Results and discussion

The frequency ratio is evaluated for nine different sets of crack parameters and a series of end mass and rotary inertia ratios for the first and second modes of vibration. Figs. 5 and 6 present the results of a crack located near the root of the beam with a location ratio of 0.1. For this crack location, two different depth ratios: 0.1 and 0.7 are considered. For each of these crack parameters, the frequency ratio r_ω is plotted as a function of rotary inertia ratio for the following four end mass ratios: 0.25, 0.50, 0.75 and 1.00. The frequency ratio is defined as

$$r_\omega = \frac{\omega(cracked)}{\omega(uncracked)}. \tag{37}$$

Figs. 7–10 present the same results for the crack location ratios 0.5 and 0.9, respectively. Figs. 11 and 12 show the mode shapes for the transverse and axial vibration for the first two modes for a crack location ratio of 0.1 and a crack depth ratio of 0.4 with and without end mass and rotary inertia. Figs. 13 and 14 show the same for crack location ratio of 0.5. Table 1 lists the dimensionless frequency parameter k_v, defined by Eq. (6), for different parameter ratio combinations and compares it to its corresponding value for the uncoupled transverse vibration case.

Upon examining Figs. 5–14 and Table 1, the following observations could be stated:

1. The frequency ratio is more sensitive to the depth ratio than to the location ratio.
2. The addition of rotary inertia increases the frequency ratios of the first mode for crack locations in the vicinity of the root. However, the frequency ratios for the second mode experienced a different trend as it tends to have high values at low rotary inertia ratio and low values at high rotary inertia ratios.
3. For cracks located in the mid-span and near the free end, the addition of rotary inertia resulted in low frequency ratios.
4. The effect of the concentrated mass on the frequency ratio is opposite in nature to that of the rotary inertia regardless to the crack location and depth ratios or the vibrational mode number.
5. An intersection point exists for all cases at which the frequency ratio is the same for a given rotary inertia ratio regardless to the mass ratio.
6. The coupling between the transverse and axial vibrations is weak for the first two modes as shown in the mode shape plots. Even with end mass and rotary inertia the coupling remains weak. This is true as long as that the aspect ratio used is 10 or more. However, the coupling effect is apparently stronger for high values of crack depth ratio as observed when comparing Figs. 13 and 14. Stronger coupling may exist for lower values of aspect ratio, but for these cases the Timoshenko beam theory should be applied for accurate modelling.
7. The weak coupling is manifested in the results of the frequency parameter k_v where the values for coupled and uncoupled cases are practically the same as seen in Table 1.

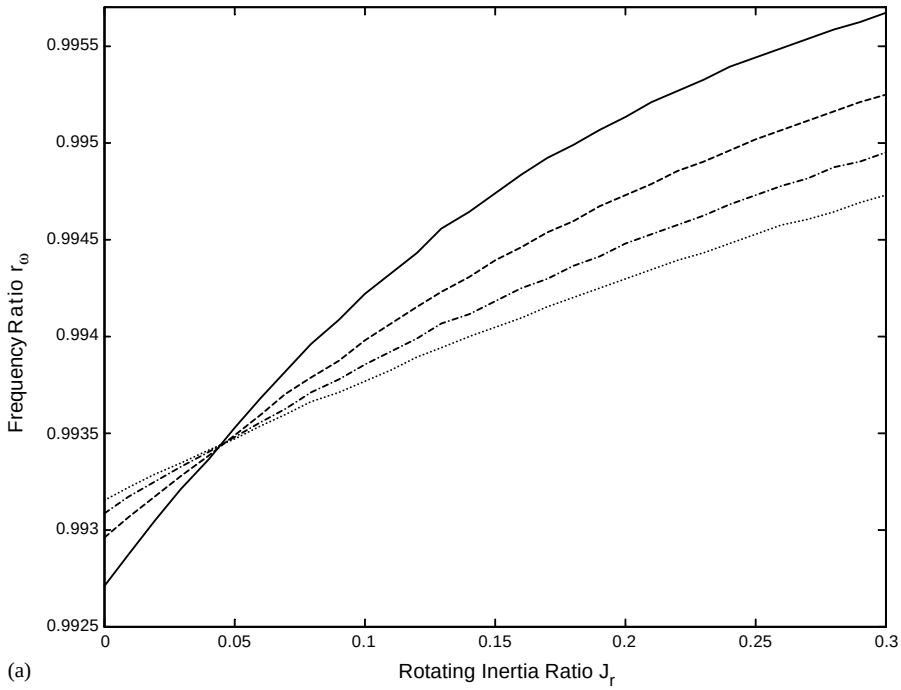

(a)

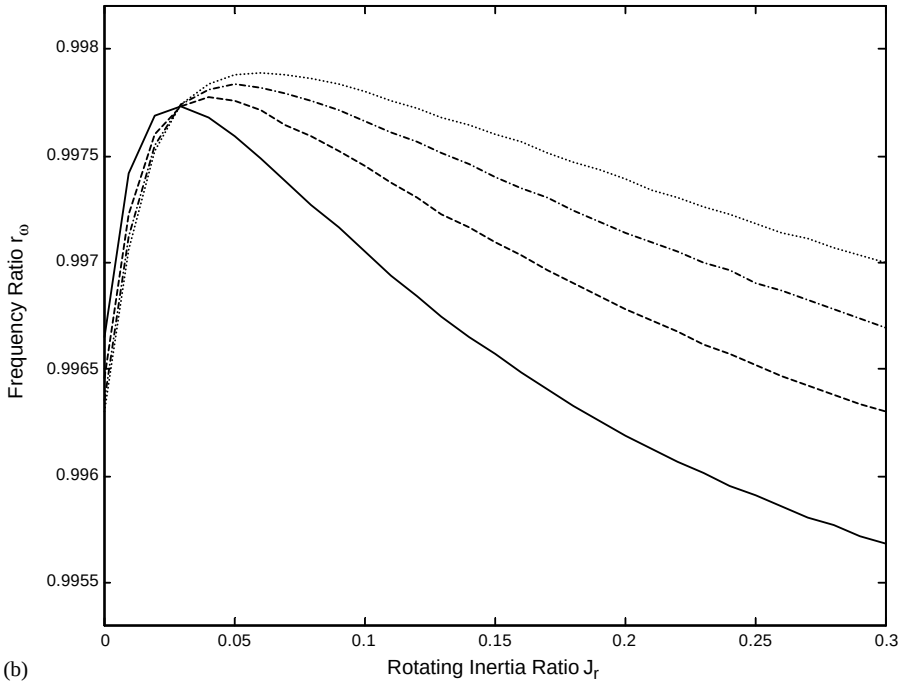

(b)

Fig. 5. Rotating inertia ratio versus the frequency ratio with crack location ratio $\bar{x}_c = 0.1$ and depth ratio $\bar{a} = 0.1$ for different mass ratios M_r: (a) first mode with different mass ratios ___ 0.25, _ _ _ 0.50, _. _. 0.75, …..1.00. (b) Second mode with different mass ratios ___ 0.25, _ _ _ 0.50, _. _. 0.75, …..1.00.

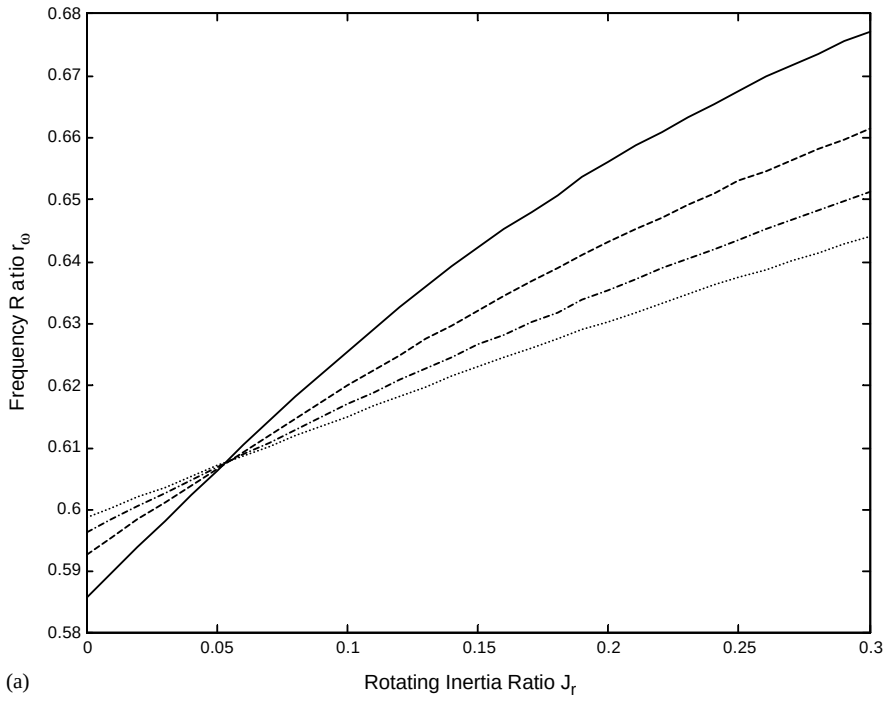

(a)

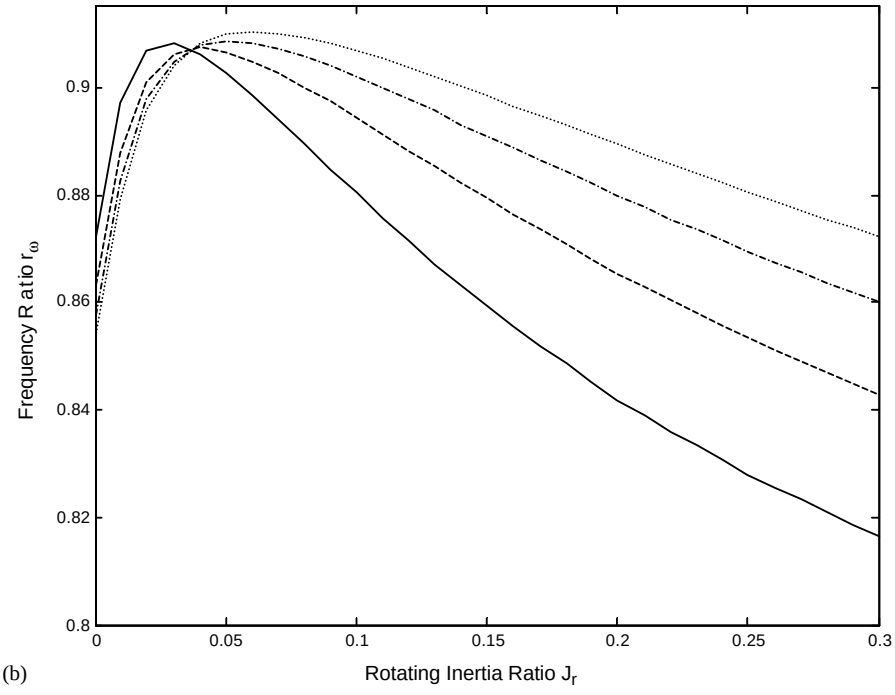

(b)

Fig. 6. Rotating inertia ratio versus the frequency ratio with crack location ratio $\bar{x}_c = 0.1$ and depth ratio $\bar{a} = 0.7$ for different mass ratio M_r: (a) first mode with different mass ratios ___ 0.25, _ _ _ 0.50, _. _. 0.75, …..1.00. (b) Second mode with different mass ratios ___ 0.25, _ _ _ 0.50, _. _. 0.75, …..1.00.

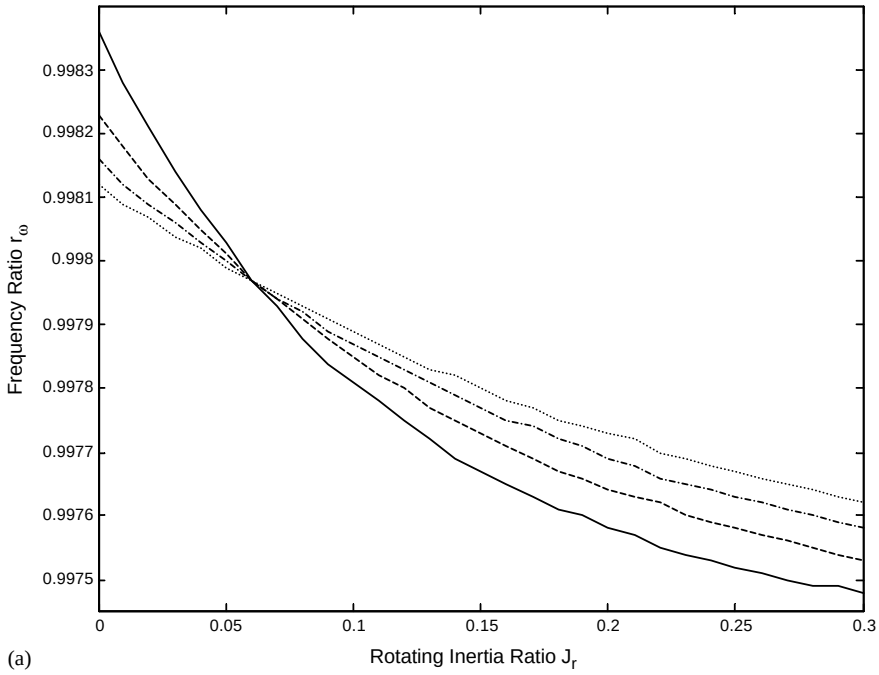

(a)

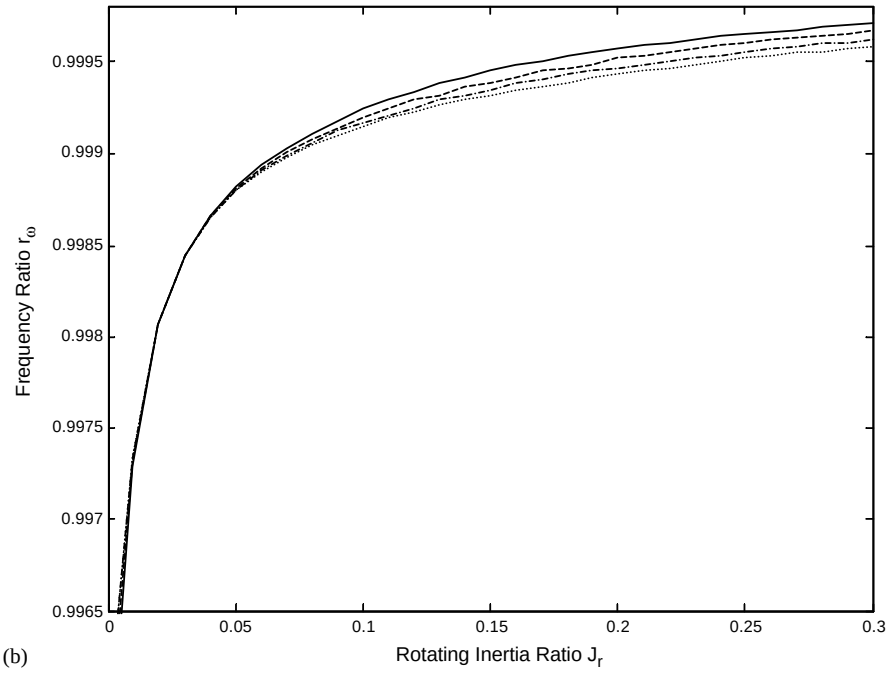

(b)

Fig. 7. Rotating inertia ratio versus the frequency ratio with crack location ratio $\bar{x}_c = 0.5$ and depth ratio $\bar{a} = 0.1$ for different mass ratio M_r: (a) first mode with different mass ratios ___ 0.25, _ _ _ 0.50, _. _. 0.75, …..1.00. (b) Second mode with different mass ratios ___ 0.25, _ _ _ 0.50, _. _. 0.75, …..1.00.

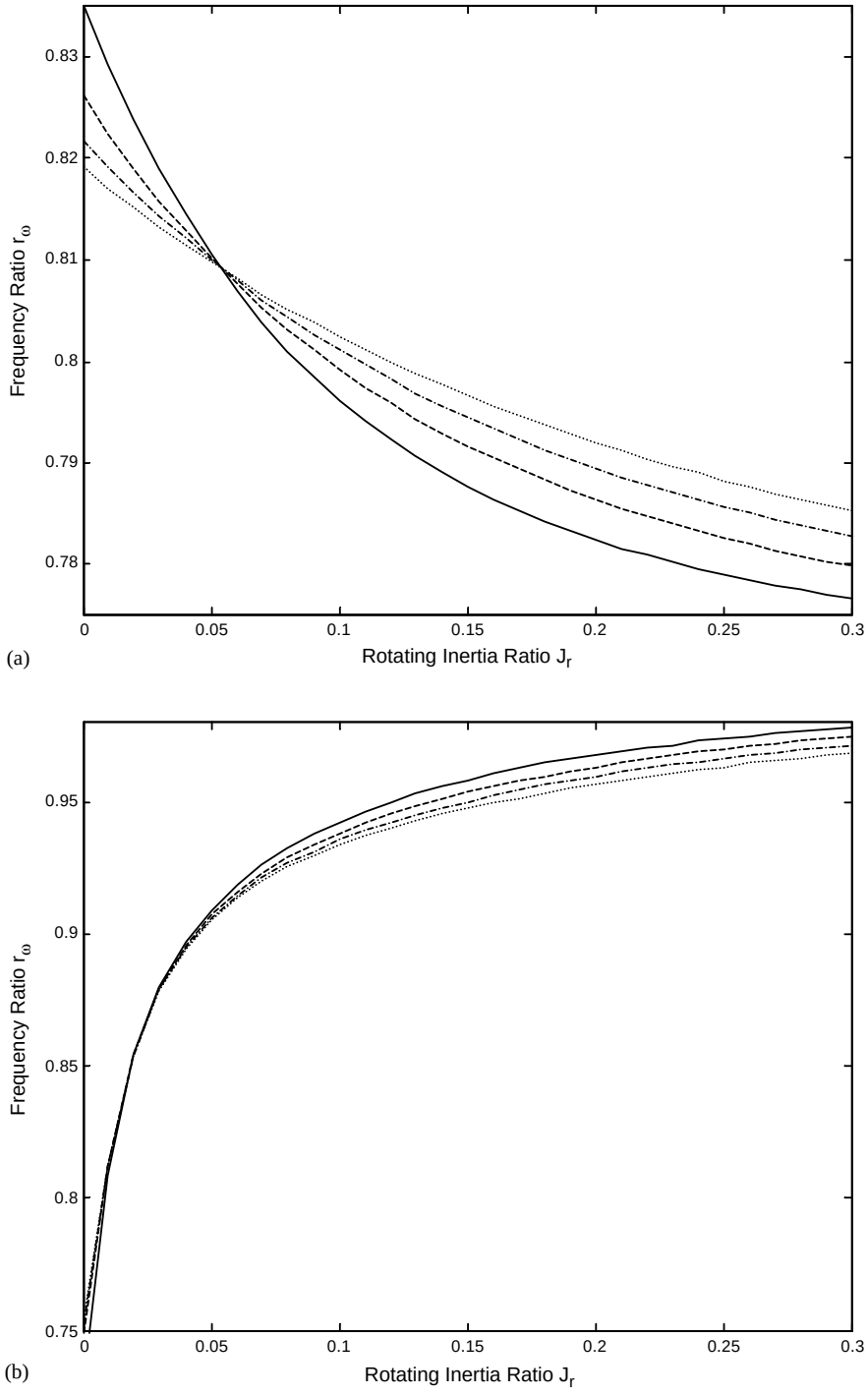

Fig. 8. Rotating inertia ratio versus the frequency ratio with crack location ratio $\bar{x}_c = 0.5$ and depth ratio $\bar{a} = 0.7$ for different mass ratio M_r: (a) first mode with different mass ratios ___ 0.25, _ _ _ 0.50, _. _. 0.75, …..1.00. (b) Second mode with different mass ratios ___ 0.25, _ _ _ 0.50, _. _. 0.75, …..1.00.

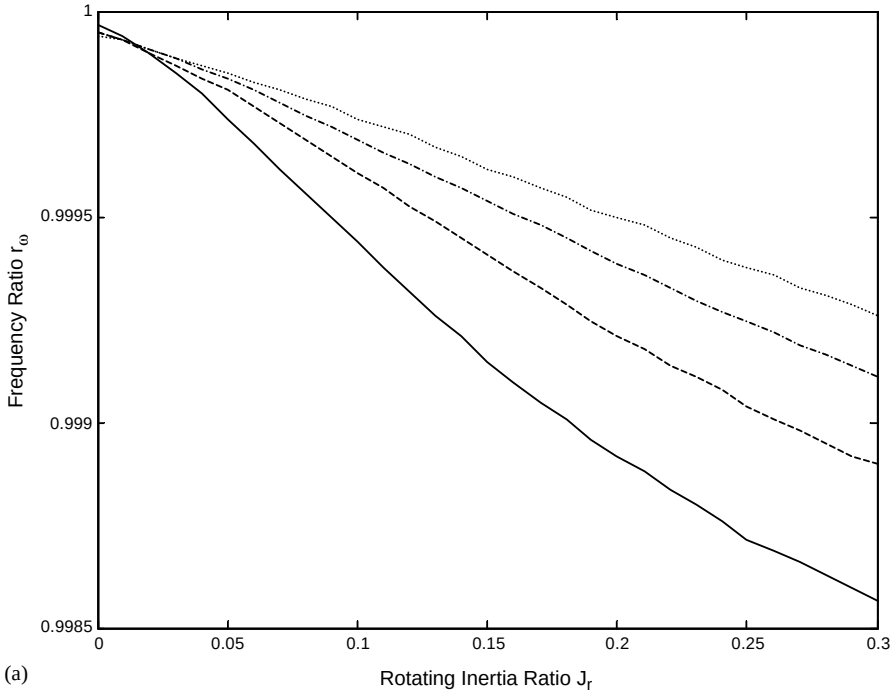

(a)

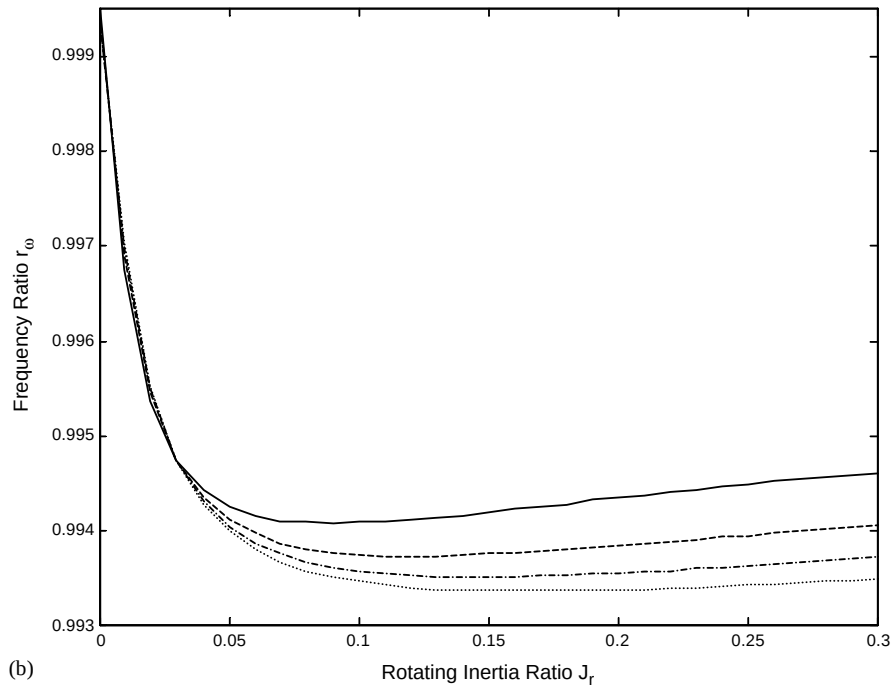

(b)

Fig. 9. Rotating inertia ratio versus the frequency ratio with crack location ratio $\bar{x}_c = 0.9$ and depth ratio $\bar{a} = 0.1$ for different mass ratio M_r: (a) first mode with different mass ratios ___ 0.25, _ _ _ 0.50, _. _. 0.75, …..1.00. (b) Second mode with different mass ratios ___ 0.25, _ _ _ 0.50, _. _. 0.75, …..1.00.

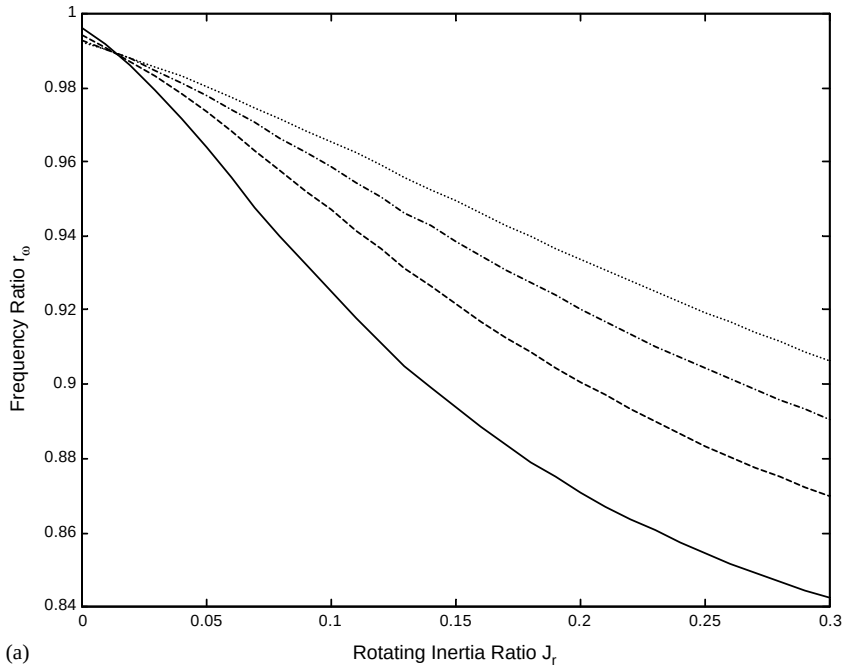

(a)

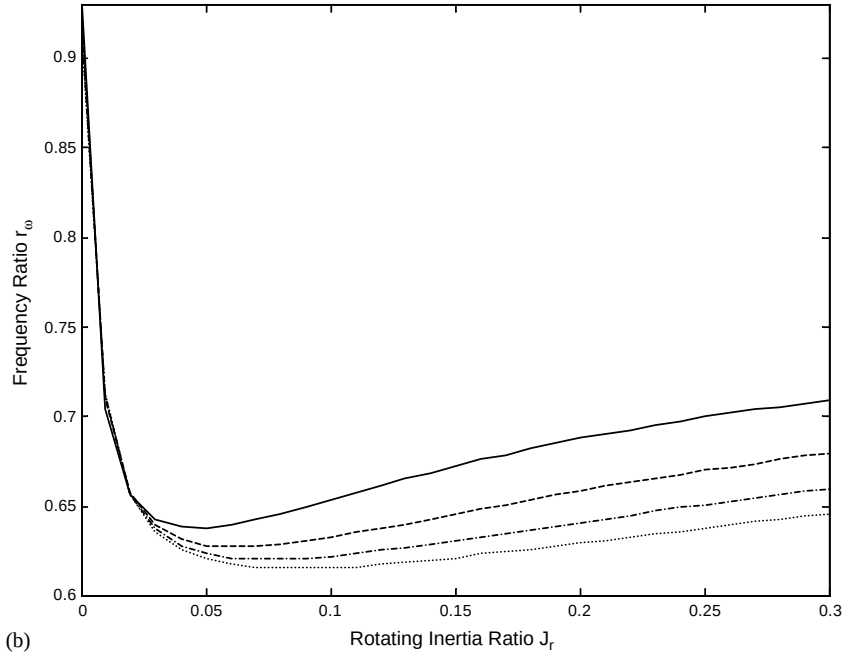

(b)

Fig. 10. Rotating inertia ratio versus the frequency ratio with crack location ratio $\bar{x}_c = 0.9$ and depth ratio $\bar{a} = 0.7$ for different mass ratio M_r: (a) first mode with different mass ratios ___ 0.25, _ _ _ 0.50, _. _. 0.75, …..1.00. (b) Second mode with different mass ratios ___ 0.25, _ _ _ 0.50, _. _. 0.75, …..1.00.

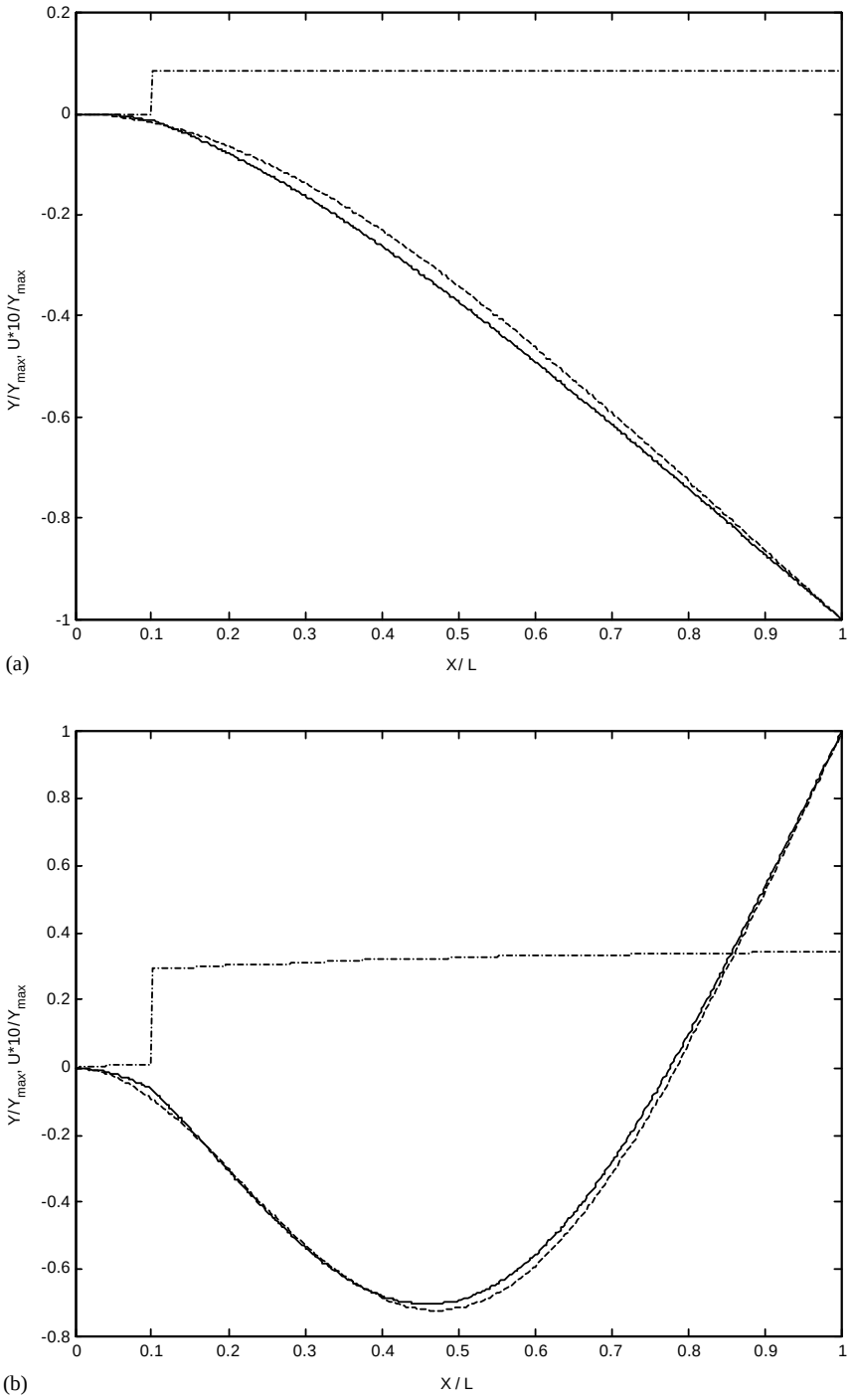

Fig. 11. Transverse and axial mode shapes with crack location ratio $\bar{x}_c = 0.1$ and depth ratio $\bar{a} = 0.4$ for the first two modes: (a) first mode, $M_r = 0$, $J_r = 0$, _._. axial cracked, _ _ _ transverse uncracked, ____ transverse cracked. (b) Second mode, $M_r = 0$, $J_r = 0$, _._. axial cracked, _ _ _ transverse uncracked, ____ transverse cracked.

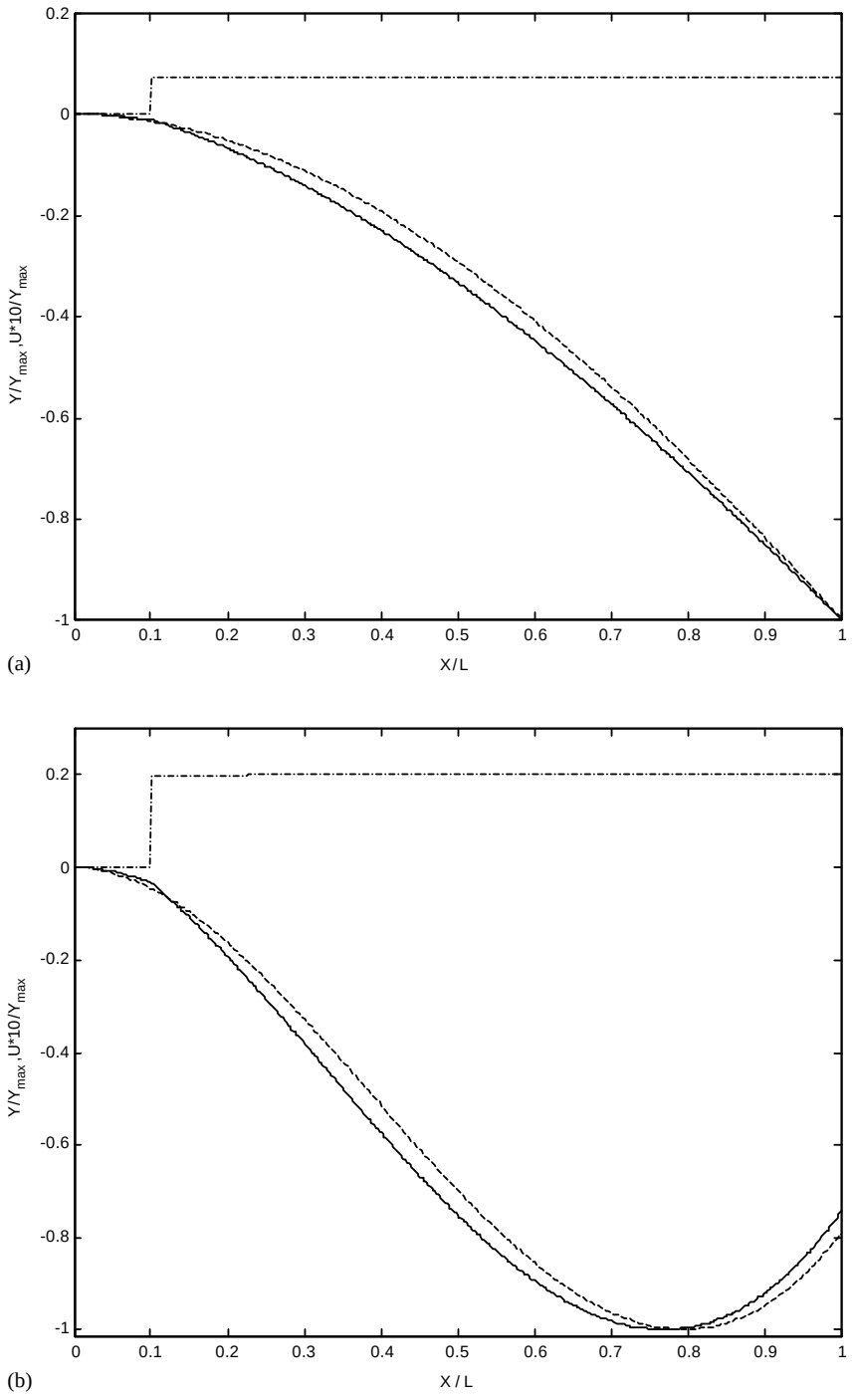

Fig. 12. Transverse and axial mode shapes with crack location ratio $\bar{x}_c = 0.1$ and depth ratio $\bar{a} = 0.4$ for the first two modes: (a) first mode, $M_r = 1.0$, $J_r = 0.3$, _._. axial cracked, _ _ _ transverse uncracked, ___ transverse cracked. (b) Second mode, $M_r = 1.0$, $J_r = 0.3$, _._. axial cracked, _ _ _ transverse uncracked, ___ transverse cracked.

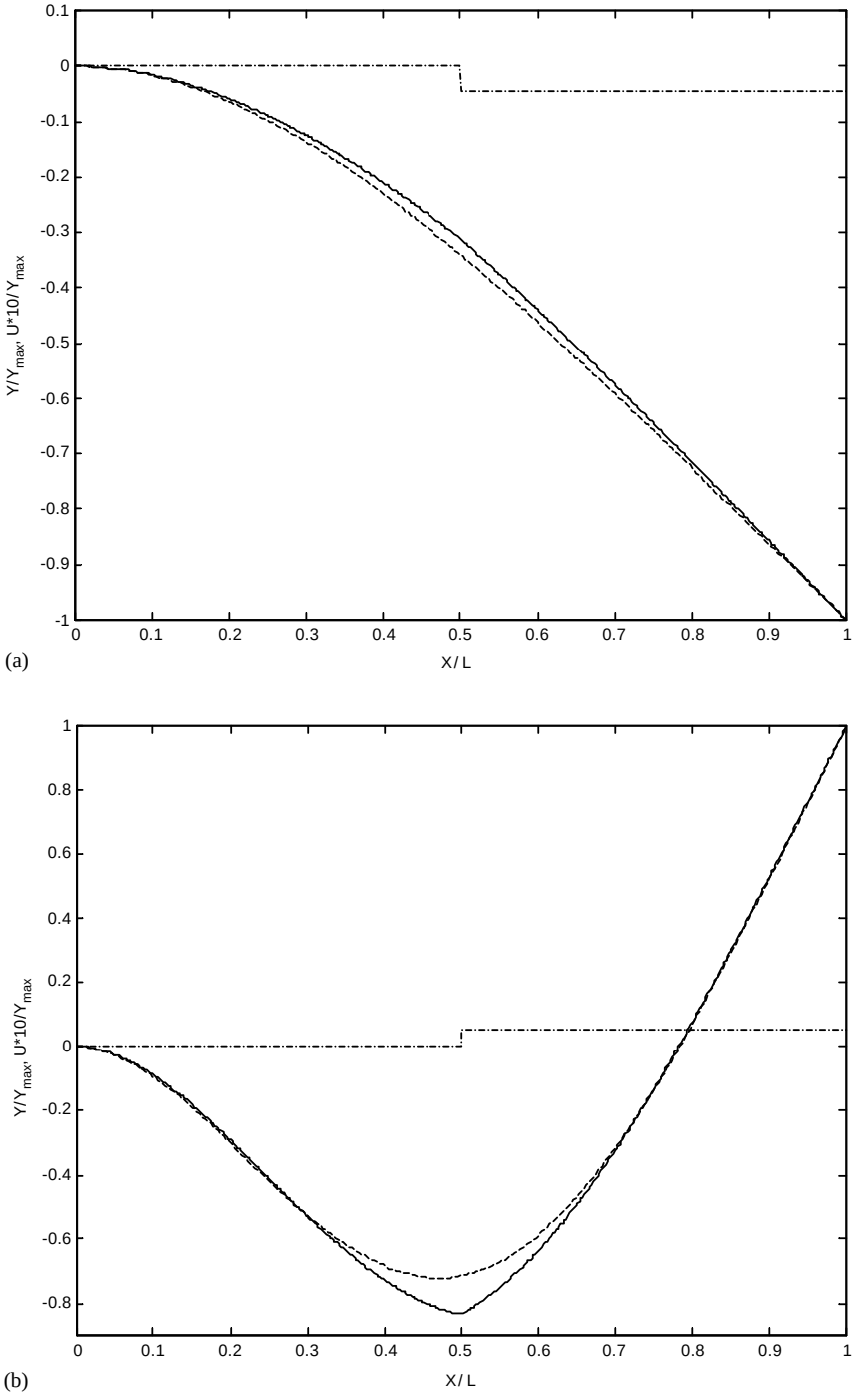

Fig. 13. Transverse and axial mode shapes with crack location ratio $\bar{x}_c = 0.5$ and depth ratio $\bar{a} = 0.4$ for the first two modes: (a) first mode, $M_r = 0$, $J_r = 0$, _._. axial cracked, _ _ _ transverse uncracked, ___ transverse cracked. (b) Second mode, $M_r = 0$, $J_r = 0$, _._. axial cracked, _ _ _ transverse uncracked, ___ transverse cracked.

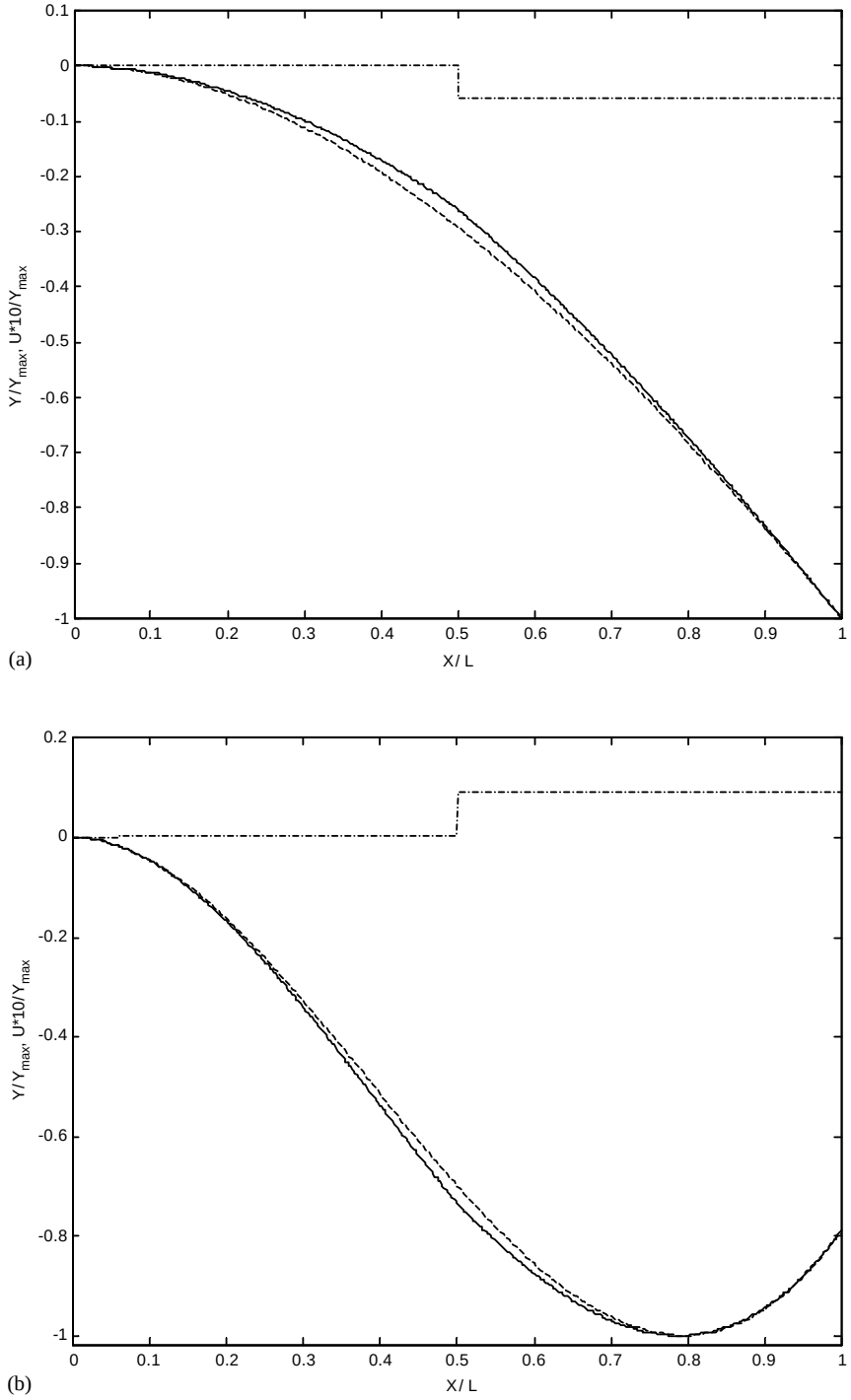

Fig. 14. Transverse and axial mode shapes with crack location ratio $\bar{x}_c = 0.5$ and depth ratio $\bar{a} = 0.4$ for the first two modes: (a) first mode, $M_r = 1.0$, $J_r = 0.3$, _._. axial cracked, _ _ _ transverse uncracked, ___ transverse cracked. (b) Second mode, $M_r = 1.0$, $J_r = 0.3$, _._. axial cracked, _ _ _ transverse uncracked, ___ transverse cracked.

Table 1
Frequency parameter for different crack parameters and end mass and rotary inertia

Crack location	Crack depth	End mass = 0.0, Rotary inertia = 0.0				End mass = 1.0, Rotary inertia = 0.3			
		First mode		Second mode		First mode		Second mode	
		Coupled	Uncoupled	Coupled	Uncoupled	Coupled	Uncoupled	Coupled	Uncoupled
0.1	0.4	1.7067	1.7068	4.5644	4.5682	1.0381	1.0381	2.0177	2.0178
	0.7	1.3123	1.3132	4.3864	4.4172	0.83385	0.83402	1.9251	1.9264
0.5	0.4	1.8432	1.8432	4.3968	4.4018	1.0745	1.0745	2.0696	2.0697
	0.7	1.6921	1.6929	3.7030	3.7526	0.94022	0.94039	2.0387	2.0394
0.9	0.4	1.8750	1.8750	4.6879	4.6879	1.0974	1.0974	1.9278	1.9279
	0.7	1.8745	1.8745	4.6454	4.6487	1.0303	1.0304	1.5949	1.5966

6. Conclusions

An investigation of the vibratory behaviour has been conducted for a cracked cantilever beam. The analysis procedure coupled the transverse and axial vibration through the crack model. The effects of end mass and rotary inertia are studied for different crack conditions. It is seen that the frequency ratio follows predictable trends in relation to the crack parameters and end mass and rotary inertia. The coupling effects between the transverse and axial vibrations observed to be weak for the first two modes. It is recommended that this investigation should be followed by applying Timoshenko beam theory to further investigate the coupling effects for short thick beams.

Appendix A

The characteristics equation $|B| = 0$.
The non-zero elements of $[B]$ matrix are:

$$B_{1,1} = 1, B_{2,3} = 1, B_{2,5} = 1$$
$$B_{3,4} = 1, B_{3,6} = 1$$
$$B_{4,7} = \sin(k_u) + M_r k_u \cos(k_u)$$
$$B_{4,8} = -\cos(k_u) + M_r k_u \sin(k_u)$$
$$B_{5,9} = \sin(k_v) + M_r k_v \cos(k_v)$$
$$B_{5,10} = -\cos(k_v) + M_r k_v \sin(k_v)$$
$$B_{5,11} = \sinh(k_v) + M_r k_v \cosh(k_v)$$
$$B_{5,12} = \cosh(k_v) + M_r k_v \sinh(k_v)$$
$$B_{6,9} = -\cos(k_v) + J_r k_v^3 \sin(k_v)$$
$$B_{6,10} = -\sin(k_v) + J_r k_v^3 \cos(k_v)$$
$$B_{6,11} = \cosh(k_v) - J_r k_v^3 \sinh(k_v)$$
$$B_{6,12} = \sinh(k_v) - J_r k_v^3 \cosh(k_v)$$
$$B_{7,1} = -\sin(k_u \bar{x}_c)$$
$$B_{7,2} = \cos(k_u \bar{x}_c)$$
$$B_{10,3} = -\sin(k_v \bar{x}_c)$$
$$B_{10,4} = \cos(k_v \bar{x}_c)$$
$$B_{10,5} = -\sinh(k_v \bar{x}_c)$$
$$B_{10,6} = -\cosh(k_v \bar{x}_c)$$
$$B_{10,9} = \sin(k_v \bar{x}_c)$$
$$B_{10,10} = -\cos(k_v \bar{x}_c)$$
$$B_{10,11} = \sinh(k_v \bar{x}_c)$$
$$B_{10,12} = \cosh(k_v \bar{x}_c)$$
$$B_{11,1} = -k_u \sin(k_u \bar{x}_c) + \bar{k}_{11}(L/h) \cos(k_u \bar{x}_c)$$
$$B_{11,2} = k_u \cos(k_u \bar{x}_c) + \bar{k}_{11}(L/h) \sin(k_u \bar{x}_c)$$
$$B_{11,3} = -k_v \bar{k}_{12} \sin(k_v \bar{x}_c)$$
$$B_{11,4} = k_v \bar{k}_{12} \cos(k_v \bar{x}_c)$$
$$B_{11,5} = k_v \bar{k}_{12} \sinh(k_v \bar{x}_c)$$
$$B_{11,6} = k_v \bar{k}_{12} \cosh(k_v \bar{x}_c)$$

$$B_{7,7} = \sin(k_u\bar{x}_c) \qquad B_{11,7} = -\bar{k}_{11}(L/h)\cos(k_u\bar{x}_c)$$
$$B_{7,8} = -\cos(k_u\bar{x}_c) \qquad B_{11,8} = -\bar{k}_{11}(L/h)\sin(k_u\bar{x}_c)$$
$$B_{8,3} = \cos(k_v\bar{x}_c) \qquad B_{11,9} = k_v\bar{k}_{12}\sin(k_v\bar{x}_c)$$
$$B_{8,4} = \sin(k_v\bar{x}_c) \qquad B_{11,10} = -k_v\bar{k}_{12}\cos(k_v\bar{x}_c)$$
$$B_{8,5} = \cosh(k_v\bar{x}_c) \qquad B_{11,11} = -k_v\bar{k}_{12}\sinh(k_v\bar{x}_c)$$
$$B_{8,6} = \sinh(k_v\bar{x}_c) \qquad B_{11,12} = -k_v\bar{k}_{12}\cosh(k_v\bar{x}_c)$$
$$B_{8,9} = -\cos(k_v\bar{x}_c) \qquad B_{12,1} = \bar{k}_{12}\cos(k_u\bar{x}_c)$$
$$B_{8,10} = -\sin(k_v\bar{x}_c) \qquad B_{12,2} = \bar{k}_{12}\sin(k_u\bar{x}_c)$$
$$B_{8,11} = -\cosh(k_v\bar{x}_c) \qquad B_{12,3} = -k_v^2\cos(k_v\bar{x}_c) - k_v\bar{k}_{22}(L/h)\sin(k_v\bar{x}_c)$$
$$B_{8,12} = -\sinh(k_v\bar{x}_c) \qquad B_{12,4} = -k_v^2\sin(k_v\bar{x}_c) + k_v\bar{k}_{22}(L/h)\cos(k_v\bar{x}_c)$$
$$B_{9,3} = \cos(k_v\bar{x}_c) \qquad B_{12,5} = k_v^2\cosh(k_v\bar{x}_c) + k_v\bar{k}_{22}(L/h)\sinh(k_v\bar{x}_c)$$
$$B_{9,4} = \sin(k_v\bar{x}_c) \qquad B_{12,6} = k_v^2\sinh(k_v\bar{x}_c) + k_v\bar{k}_{22}(L/h)\cosh(k_v\bar{x}_c)$$
$$B_{9,5} = -\cosh(k_v\bar{x}_c) \qquad B_{12,7} = -\bar{k}_{21}(L/h)^2\cos(k_u\bar{x}_c)$$
$$B_{9,6} = -\sinh(k_v\bar{x}_c) \qquad B_{12,8} = -\bar{k}_{21}(L/h)^2\sin(k_u\bar{x}_c)$$
$$B_{9,9} = -\cos(k_v\bar{x}_c) \qquad B_{12,9} = k_v\bar{k}_{22}(L/h)\sin(k_v\bar{x}_c)$$
$$B_{9,10} = -\sin(k_v\bar{x}_c) \qquad B_{12,10} = -k_v\bar{k}_{22}(L/h)\cos(k_v\bar{x}_c)$$
$$B_{9,11} = \cosh(k_v\bar{x}_c) \qquad B_{12,11} = -k_v\bar{k}_{22}(L/h)\sinh(k_v\bar{x}_c)$$
$$B_{9,12} = \sinh(k_v\bar{x}_c) \qquad B_{12,12} = -k_v\bar{k}_{22}(L/h)\cosh(k_v\bar{x}_c)$$

References

[1] A. Joshi, B.S. Madhusudhan, A unified approach to free vibration of locally damaged beam having various homogeneous boundary conditions, Journal of Sound and Vibration 147 (1991) 475–488.

[2] W.T. Thompson, Vibration of slender beams with discontinuities, Journal of Applied Mechanics 16 (1949) 203–207.

[3] C.A. Papadopoulos, A.D. Dimarogonas, Coupled longitudinal and bending vibrations of a cracked shaft, Journal of Vibration and Acoustics Stress and Reliability in Design 110 (1988) 1–8.

[4] A.D. Dimarogonas, S.A. Paipeties, Analytical Methods in Rotor Dynamics, Elsevier Applied Science, London, 1983.

[5] A.D. Dimarogonas, C.A. Papadopoulos, Vibration of cracked shafts in bending, Journal of Sound and Vibration 15 (1983) 439–444.

[6] T.G. Chondros, A.D. Dimarogonas, J. Yao, A continuous cracked beam vibration theory, Journal of Sound and Vibration 215 (1998) 17–34.

[7] T.G. Chondros, A.D. Dimarogonas, Vibration of a cracked cantilever beam, Journal of Vibration and Acoustics 120 (1998) 742–746.

[8] L. Nobile, Mixed mode crack initiation and direction in beam with edge crack, Theoretical and Applied Fracture Mechanics 33 (2000) 107–116.

[9] G.C. Sih, Mechanics of Fracture Initiation and Propagation, Kluwer Academic Publisher, Boston, 1991.

[10] P.F. Rizos, N. Aspragathos, A.D. Dimarogonas, Identification of crack location and magnitude in a cantilever beam from the vibration modes, Journal of Sound and Vibration 138 (1990) 381–388.

[11] S. Christides, A.D. Barr, Design one-dimensional theory of cracked Euler–Bernoulli beam, Journal of Vibration and Acoustics Stress and Reliability 111 (1984) 81–84.

[12] M.H. Shen, C. Pierre, Natural modes of Euler–Bernoulli beams with symmetric cracks, Journal of Sound and Vibration 138 (1990) 115–134.

[13] M.D. Rajab, A. Al-Saleeh, Vibrational characteristics of cracked shaft, Journal of Sound and Vibration 147 (1991) 465–473.

[14] M.L. Kikidis, C.A. Papadopoulos, Slenderness ratio effects on cracked beam, Journal of Sound and Vibration 155 (1992) 1–11.
[15] P. Gudmundson, Eigenfrequency changes of structures due to cracks, notches or other geometrical changes, Journal of Mechanics and Physics of Solids 30 (1982) 339–353.
[16] P. Gudmundson, The dynamic behaviour of slender structures with cross-sectional cracks, Journal of Mechanics and Physics of Solids 31 (1983) 239–345.
[17] F. Ismail, A. Ibrahim, H.R. Martin, Identification of fatigue cracks from vibration testing, Journal of Sound and Vibration 140 (1990) 305–317.
[18] M.H. Dado, A comprehensive crack identification algorithm for beams under different end conditions, Applied Acoustics 51 (1997) 381–398.
[19] T.D. Chaudhari, S.K. Maiti, N.S. Atluri, Transverse vibration of geometrically segmented beams with and without crack, Computer Modeling and Simulating in Engineering 4 (1999) 260–273.
[20] M.A. Mohiuddin, Y.A. Khulief, Modal characteristics of cracked rotors using a canonical shaft finite element, Computer Methods in Applied Mechanics and Engineering 162 (1998) 223–247.
[21] S. Masoud, M.A. Jarrah, M. Al-Maamory, Effect of crack depth on the natural frequency of a prestressed fixed–fixed beam, Journal of Sound and Vibration 214 (1998) 201–212.
[22] K.-H. Kim, J.-H. Kim, Effect of a crack on the dynamic stability of free–free beam subjected to follower force, Journal of Sound and Vibration 233 (2000) 119–135.
[23] H.L. Ewalds, R.J.H. Wnahil, Fracture Mechanics, Edward Arnold and Delftse Uitgevers Maatschappij, London, 1984.